Electronic Supplementary Material (ESI) for Journal of Materials Chemistry A.

Photo-assisted asymmetric supercapacitors based on dual photoelectrodes for enhanced photoelectric energy storage

Yunbo Zhao,[a] Hui Li,*[a] Ruiyang Tang,[a] Xueyan Wang,[a] Yang Wu,*[a,b] Shi Yan[c] and Yu Zhang*[a]

[a] *College of Chemistry, Liaoning University, Shenyang 110036, China.*

[b] *Institute of antirust materials, Liaoning University, Shenyang 110036, China.*

[c] *Liaoning Inspection Examination & Certificatian Centre, Shenyang 110036, China.*

*Corresponding authors.

E-mail: lihui@lnu.edu.cn; wuyang@lnu.edu.cn; zhangy@lnu.edu.cn

Calculation Methods:

The specific capacitance (C, F g^{-1}) of the working electrode was calculated from the GCD curve according to the following equation:

$$C = \frac{I \times \Delta t}{m \times \Delta V} \qquad (1)$$

where I (A) is discharge current, Δt (s) is the discharge time, m (g) is the mass of the active materials, $\triangle V$ (V) is the potential range.

For ASC, the $ZnCo_2O_4$ nanoflowers served as the positive electrode while the negative electrode was $CuCo_2S_4$ hollow spheres.It is necessary to maintain charge (Q) balance between positive and negative electrodes according to the charge balance equation: $Q_+ = Q_-$ ($Q = m \times C \times \triangle V$). The mass ratio ($m_+/m_-$) is expressed as follows:

$$\frac{m_+}{m_-} = \frac{C_- \times \triangle V_-}{C_+ \times \triangle V_+} \qquad (2)$$

where m is the mass loading, C is the specific capacitance, and ΔV is the potential range.

In addition, the specific capacitances (C_s, F g^{-1}), coulombic efficiency (η) energy density (E, W h Kg^{-1}), and power density (P, W Kg^{-1}) were calculated using equation (3) – (6) [1]:

$$C_S = 2\frac{I \times \Delta t}{m \times \Delta V} \qquad (3)$$

$$\eta = \frac{t_d}{t_c} \times 100\% \qquad (4)$$

$$E = \frac{C_S \times (\Delta V)^2}{2 \times 3.6} \qquad (5)$$

$$P = 3600 \times \frac{E}{\Delta t} \qquad (6)$$

where I (A) is discharge current, Δt (s) and t_d (s) are the discharge time, m (g) is the mass of the active materials, $\triangle V$ (V) is the potential range, t_c (s) is the charge time.

The battery-type specific capacity (C_g, C g^{-1}) of the ASC were calculated as follows [2-4]:

$$C_g = \frac{I \times \Delta t}{m} \qquad (7)$$

where I (A) is discharge current, Δt (s) is the discharge time, m (g) is the mass of the active materials.

The specific discharge capacity (C_m, mAh g^{-1}) of the ASC were calculated as follows [5-7]:

$$C_m = \frac{I \times \Delta t}{3.6 \times m} \qquad (8)$$

where I (A) is discharge current, Δt (s) is the discharge time, m (g) is the mass of the active materials.

The adsorption energies (E_{ad}) of OH on the $ZnCo_2O_4$ [111] surfaces were calculated as [8]:

$$\Delta E_{OH^*} = E(OH^*) - E(*) - (E_{H_2O} - \tfrac{1}{2}E_{H_2}) \qquad (7)$$

where $E(OH^*)$, $E(*)$ are the total energy after OH^* adsorption and the ground state energy of the surface before OH^* adsorption. E_{H_2O} and E_{H_2} are the computed ground state energies of H_2O and H_2 molecules in the gas phase.

Table S1 Elemental compositions for Zn, Co, O of ZCO NF

C (%)	Co (%)	O (%)	Zn (%)
30.29	18.37	42.15	9.19

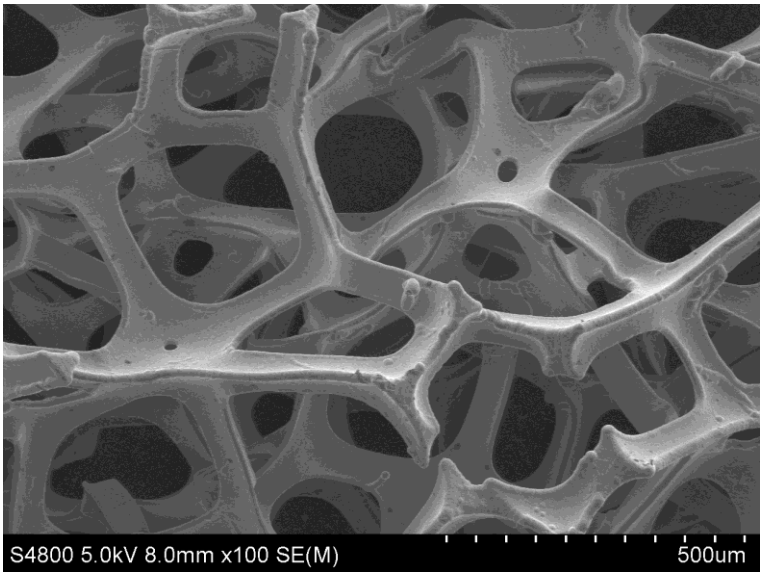

Fig. S1 SEM image of bare nickel foam.

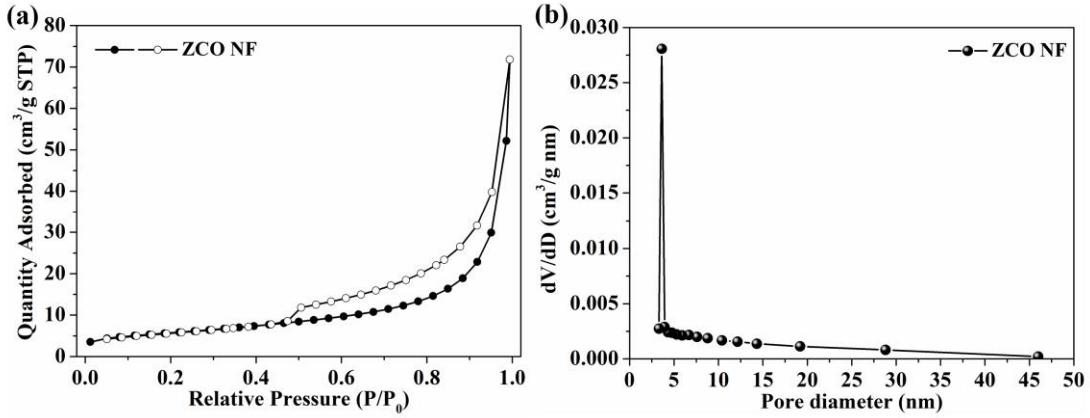

Fig. S2 (a) Nitrogen adsorption-desorption isotherms of ZCO NF. (b) The plot of pore size distribution calculated by BJH model.

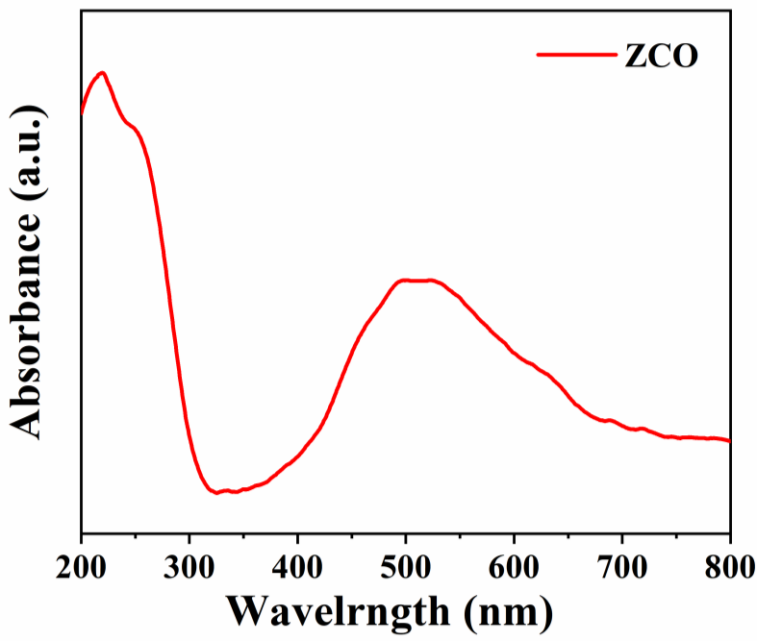

Fig. S3 UV-vis diffuse reflectance spectra of ZCO NF.

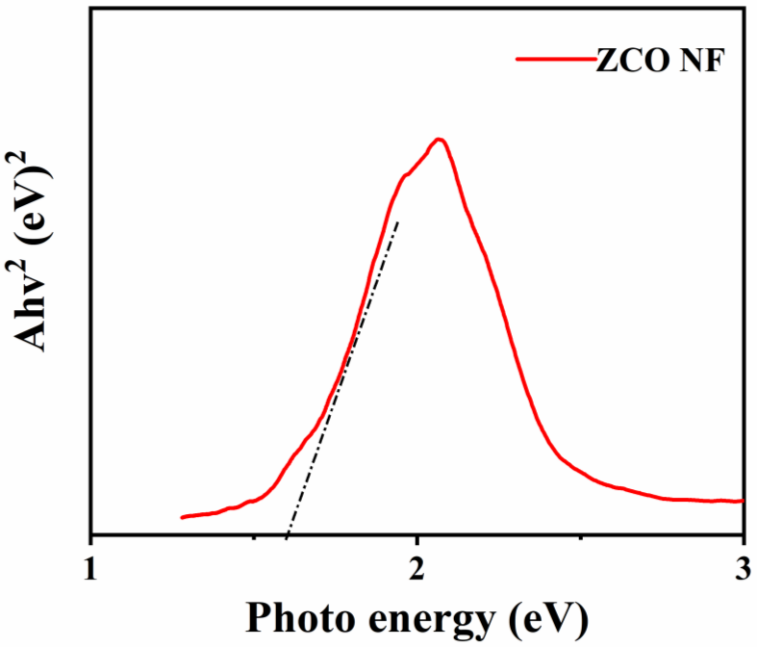

Fig. S4 Kubelka-Munk plot of ZCO NF.

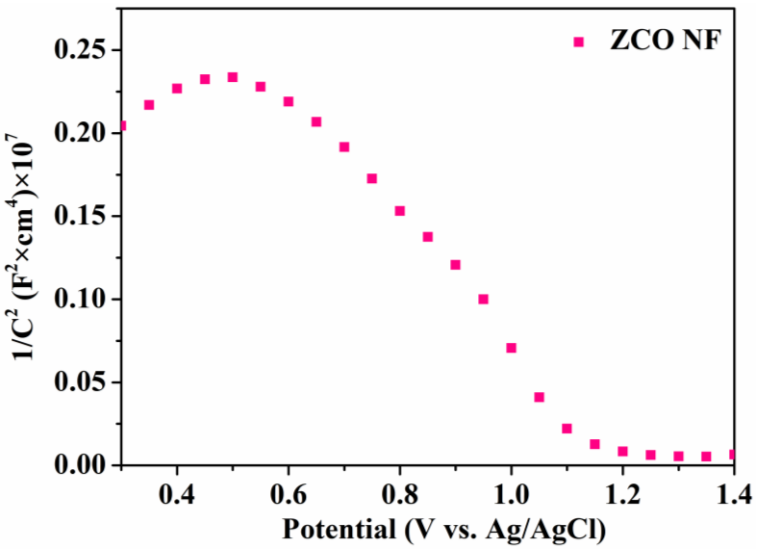

Fig. S5 Mott-Schottky plot of ZCO NF.

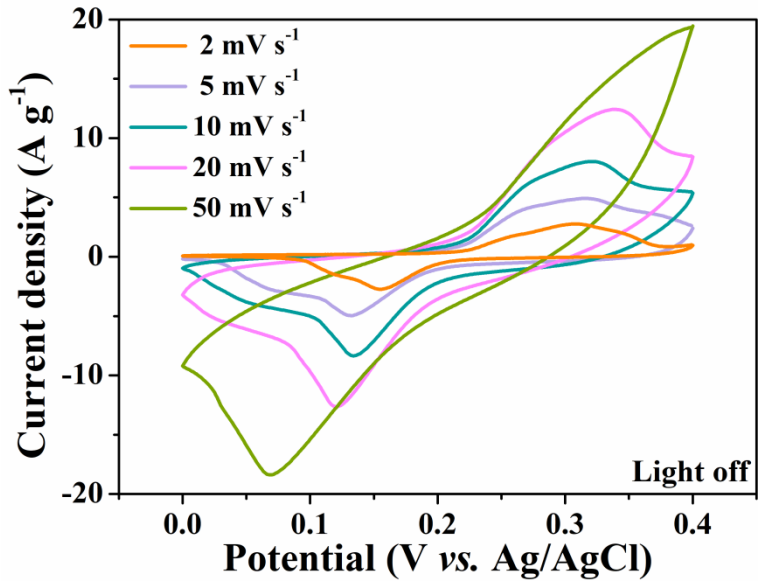

Fig. S6 CV curves for ZCO NF at different scan rates under dark condition.

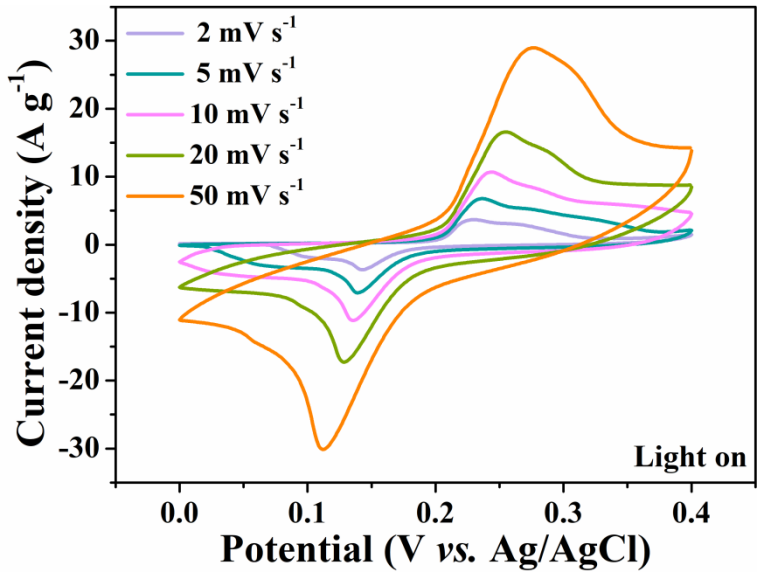

Fig. S7 CV curves for ZCO NF at different scan rates under light illumination.

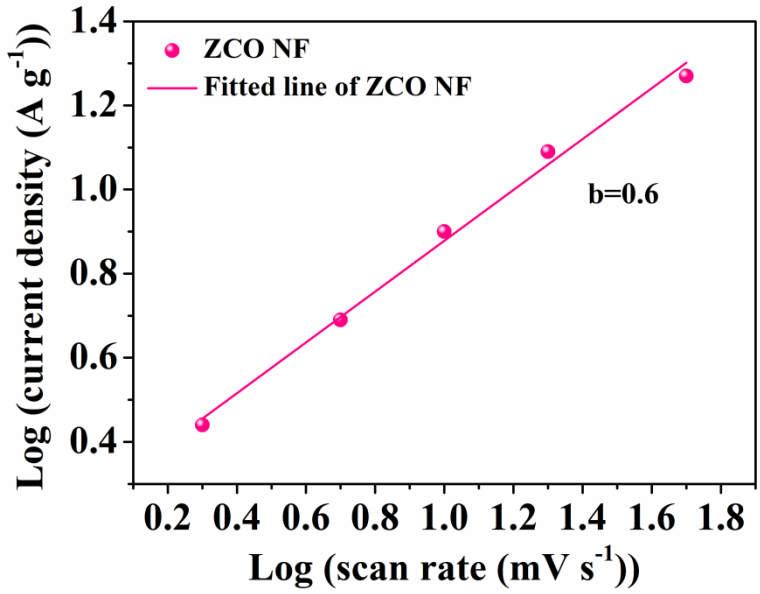

Fig. S8 The linear relation between log(i) and log(v) under dark condition.

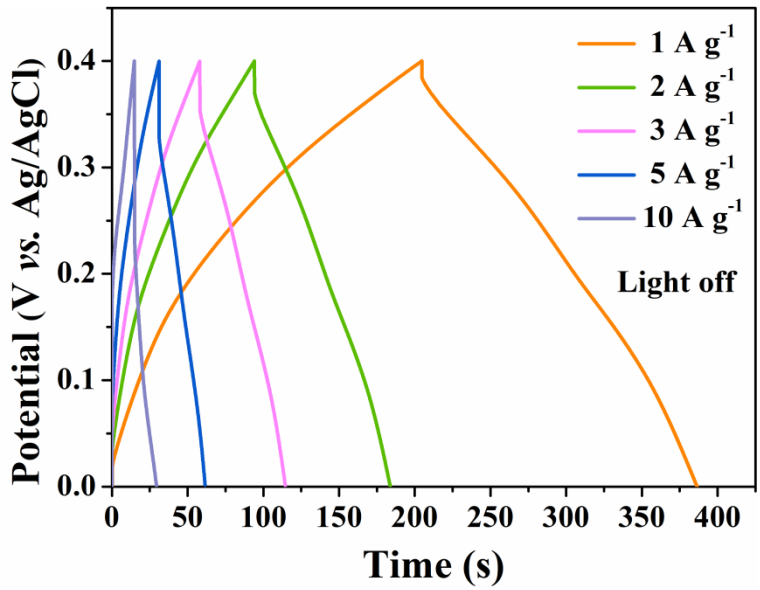

Fig. S9 GCD curves for ZCO NF at various current densities under dark condition.

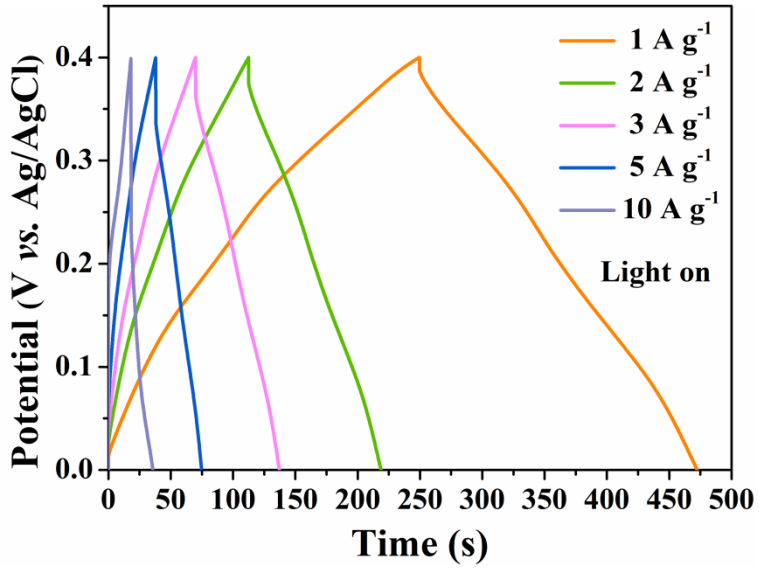

Fig. S10 GCD curves for ZCO NF at various current densities under light illumination.

Table S2 The specific capacitance of the ZCO NF positive electrodes at various current densities with and without light illumination

	1 A g^{-1}	2 A g^{-1}	3 A g^{-1}	5 A g^{-1}	10 A g^{-1}
Light on	563 F g^{-1}	532 F g^{-1}	507 F g^{-1}	463 F g^{-1}	435 F g^{-1}
Light off	456 F g^{-1}	445 F g^{-1}	425 F g^{-1}	383 F g^{-1}	363 F g^{-1}

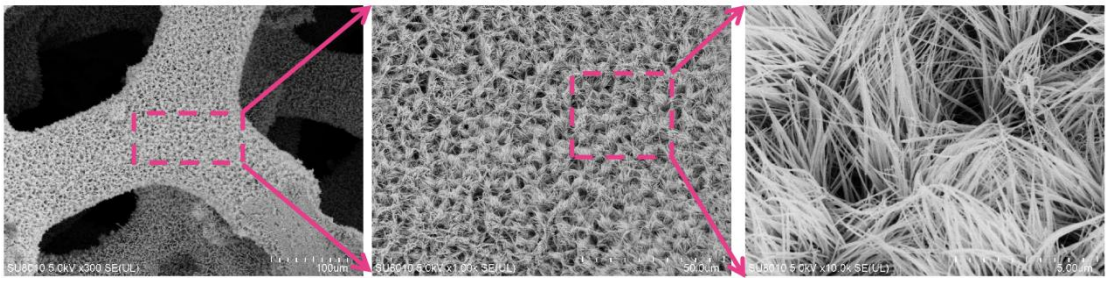

Fig. S11 Low- and high-magnification SEM images of ZCO NNF.

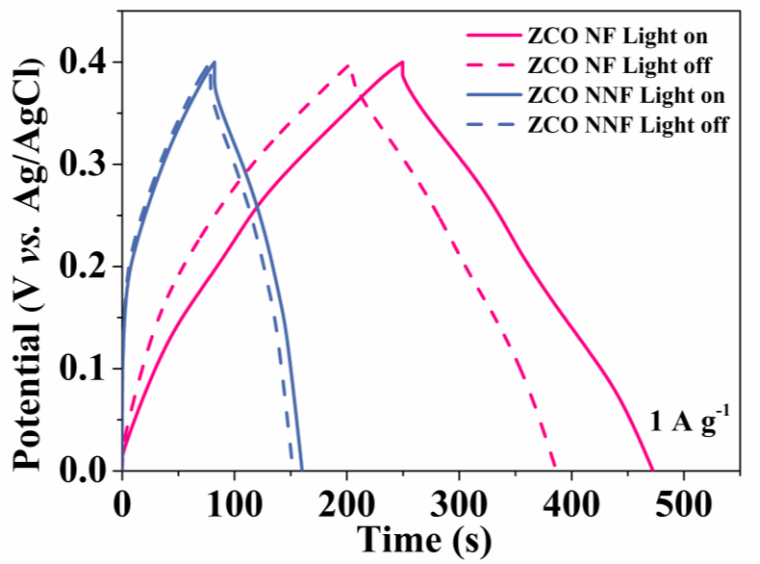

Fig. S12 GCD curves for ZCO NF and ZCO NNF at 1 A g^{-1} with and without light.

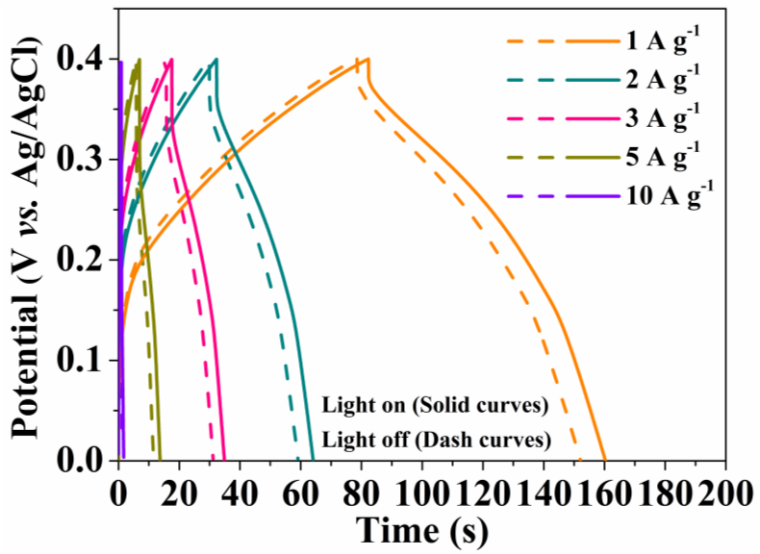

Fig. S13 GCD curves for the ZCO NNF at different current densities under dark (dash curves) and light (solid curves).

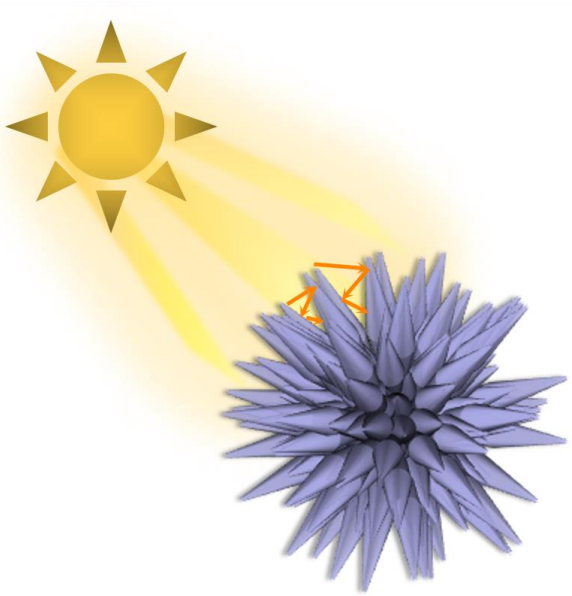

Scheme S1 Schematic illustration of multi-absorption within ZCO NF.

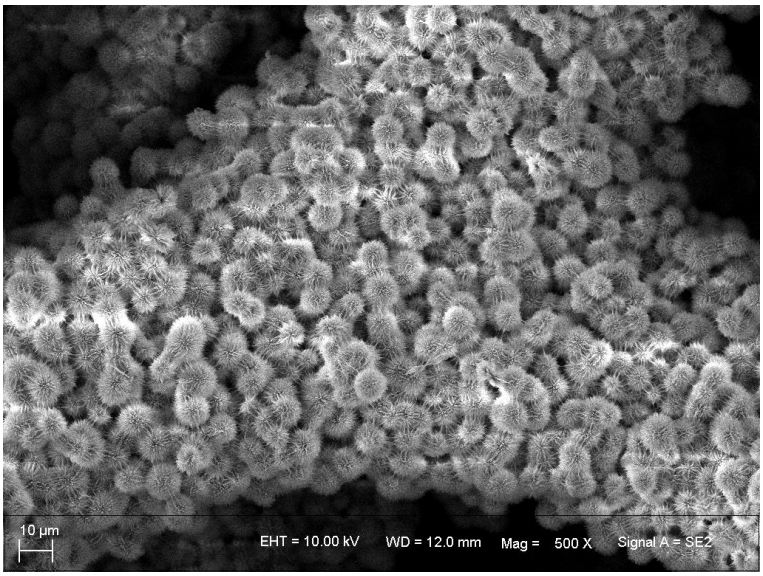

Fig. S14 Low-magnification SEM images of $CuCo_2O_4$.

Fig. S15 High-magnification SEM image of $CuCo_2O_4$.

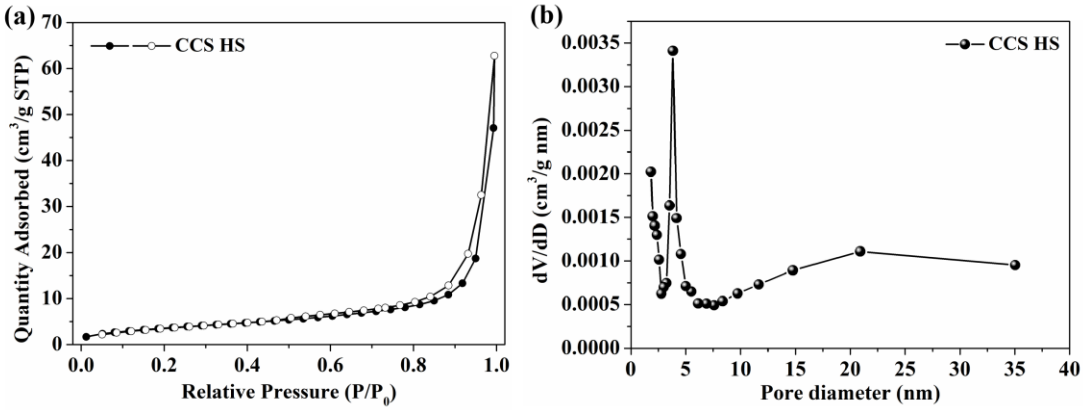

Fig. S16 (a) Nitrogen adsorption-desorption isotherms of CCS HS. (b) The plot of pore size distribution calculated by BJH model.

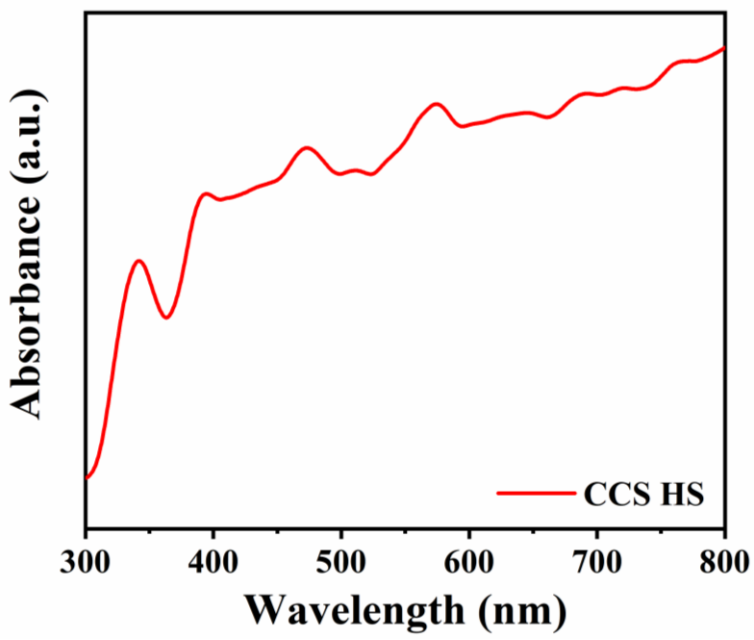

Fig. S17 UV-vis diffuse reflectance spectra of CCS HS.

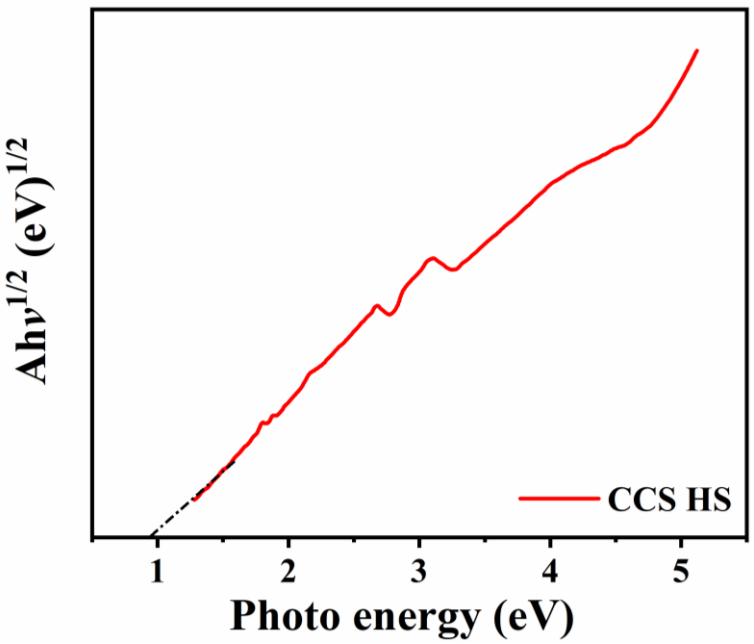

Fig. S18 Kubelka-Munk plots of CCS HS.

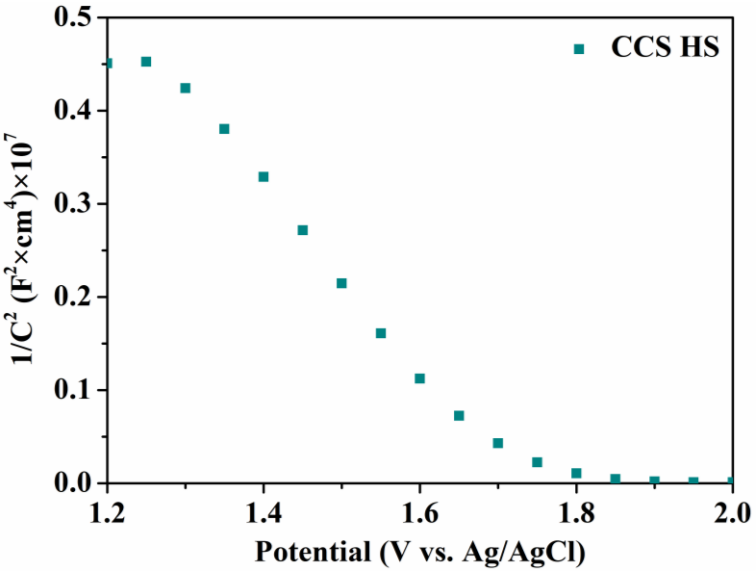

Fig. S19 Mott-Schottky plot of CCS HS.

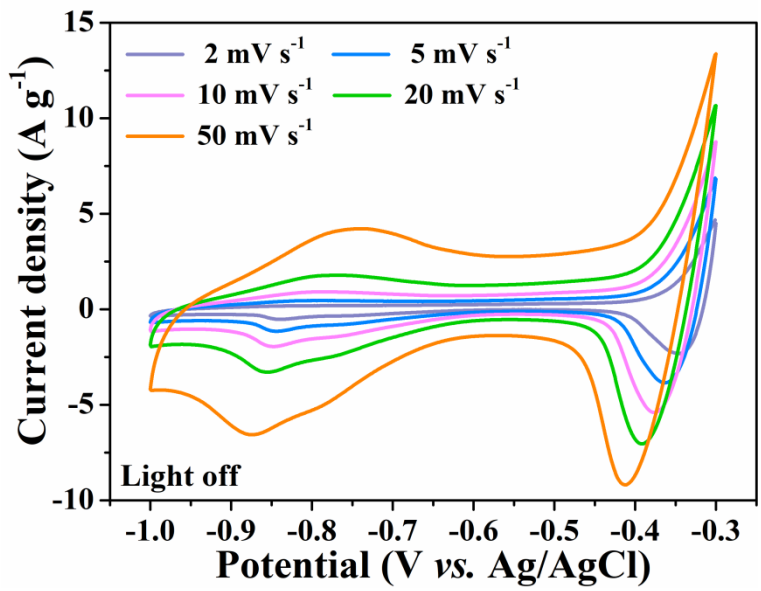

Fig. S20 CV curves for CCS HS at different scan rates under dark condition.

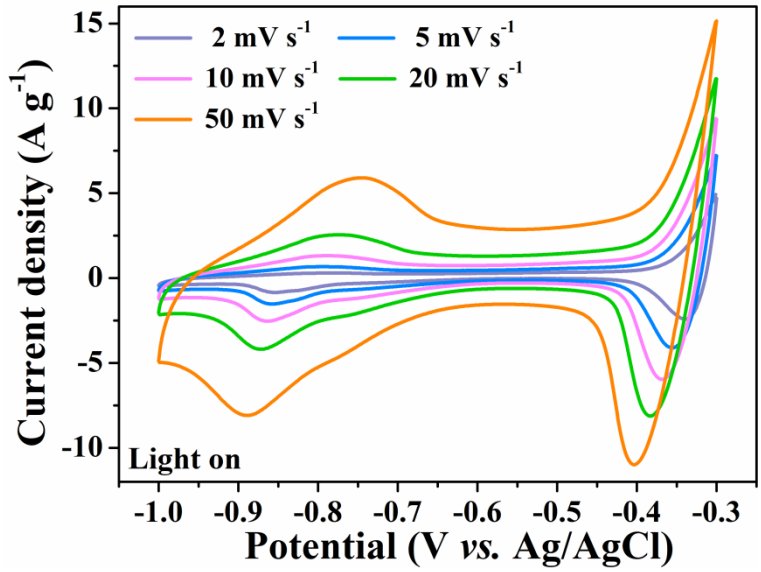

Fig. S21 CV curves for CCS HS at different scan rates under light illumination.

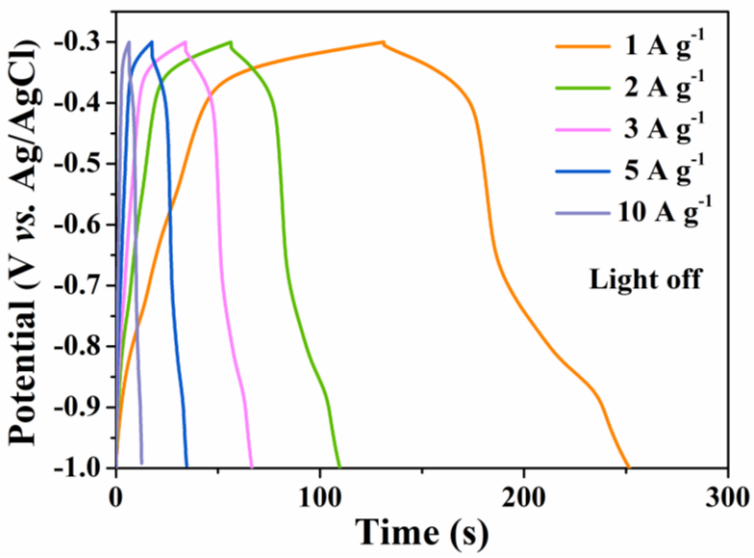

Fig. S22 GCD curves for CCS HS at various current densities under dark condition.

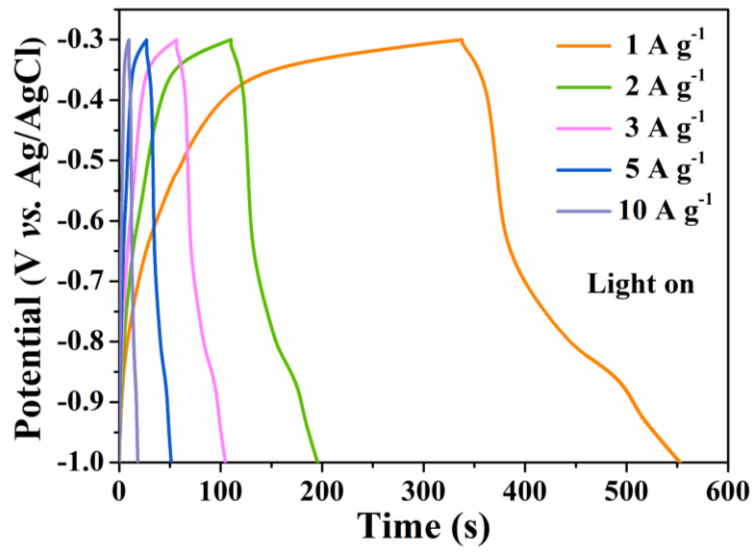

Fig. S23 GCD curves for CCS HS at various current densities under light illumination.

Table S3 The specific capacitance of the CCS HS negative electrodes at various current densities with and without light illumination

	1 A g^{-1}	2 A g^{-1}	3 A g^{-1}	5 A g^{-1}	10 A g^{-1}
Light on	305 F g^{-1}	245 F g^{-1}	208 F g^{-1}	174 F g^{-1}	127 F g^{-1}
Light off	174 F g^{-1}	155 F g^{-1}	141 F g^{-1}	123 F g^{-1}	90 F g^{-1}

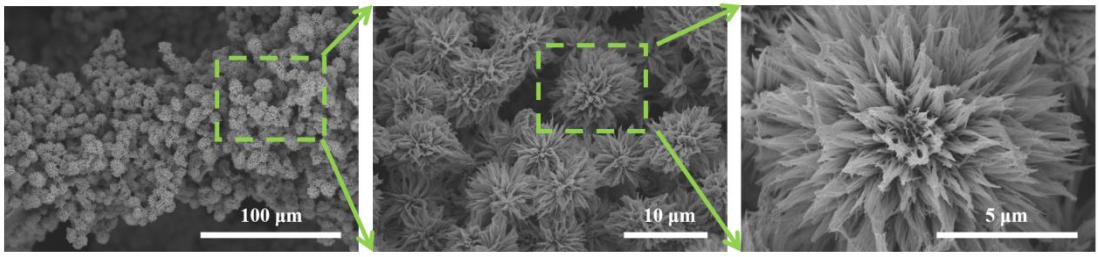

Fig. S24 Low- and high-magnification SEM images of CCS NHS.

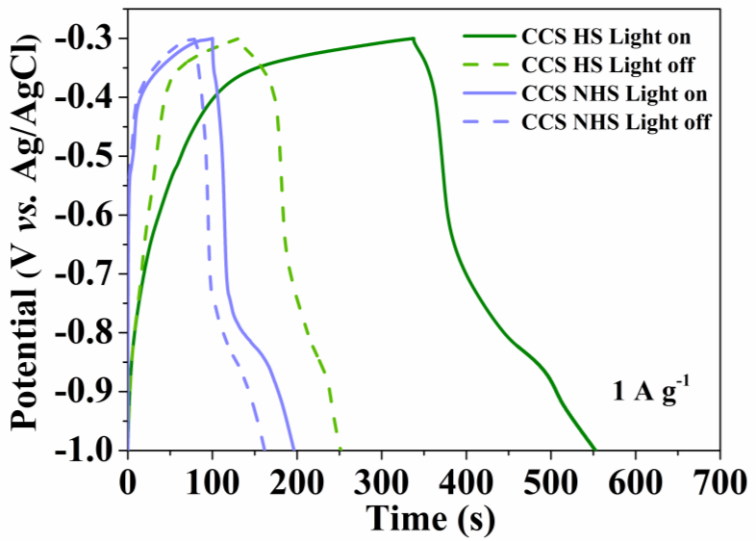

Fig. S25 GCD curves for CCS HS and CCS NHS at 1 A g^{-1} with and without light.

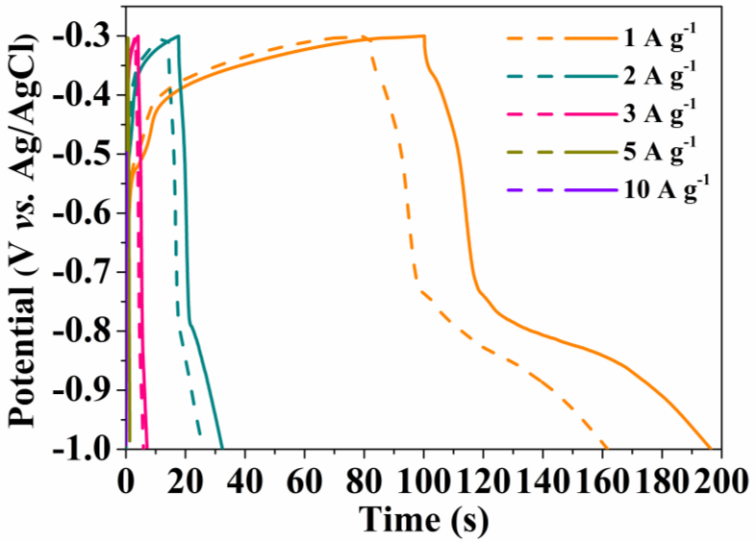

Fig. S26 GCD curves for the CCS NHS at different current densities under dark (dash curves) and light (solid curves).

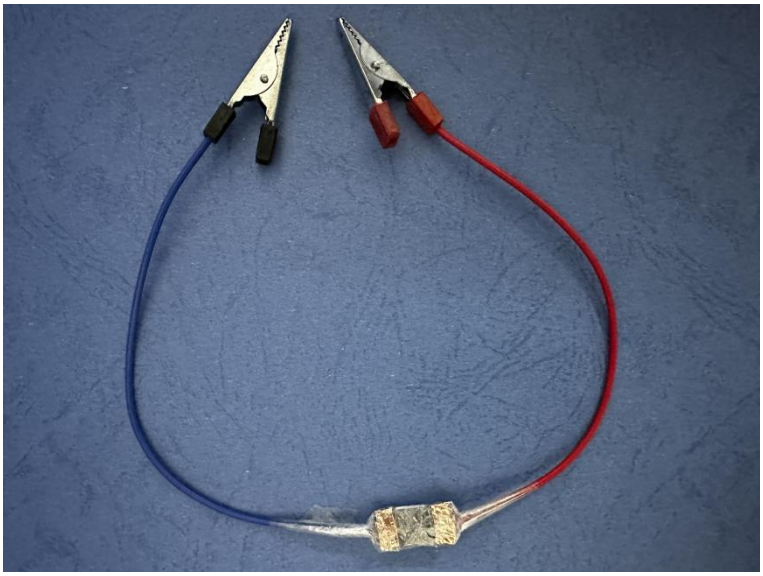

Fig. S27 The photo of ZCO NF//CCS HS ASC.

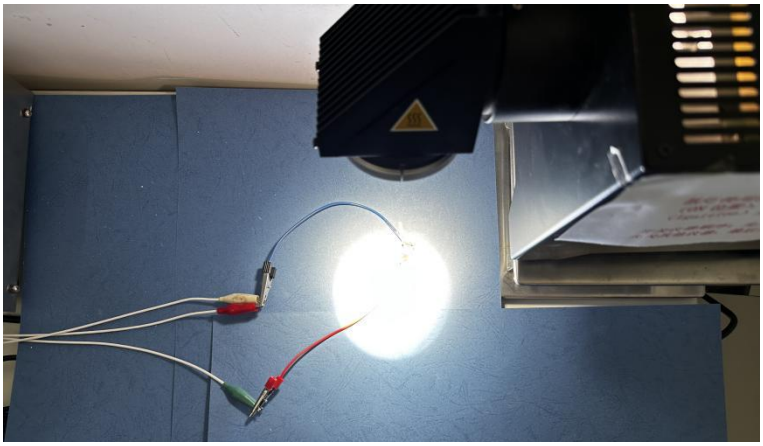

Fig. S28 The photo of photo-assisted ZCO NF//CCS HS ASC.

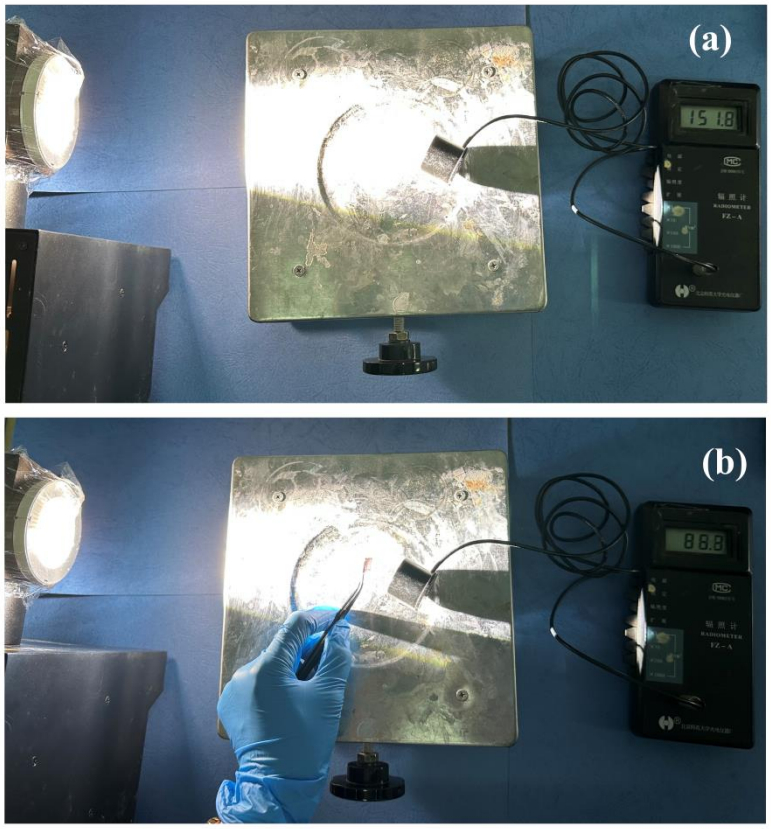

Fig. S29 Photo of the radiometer measuring the light intensity.

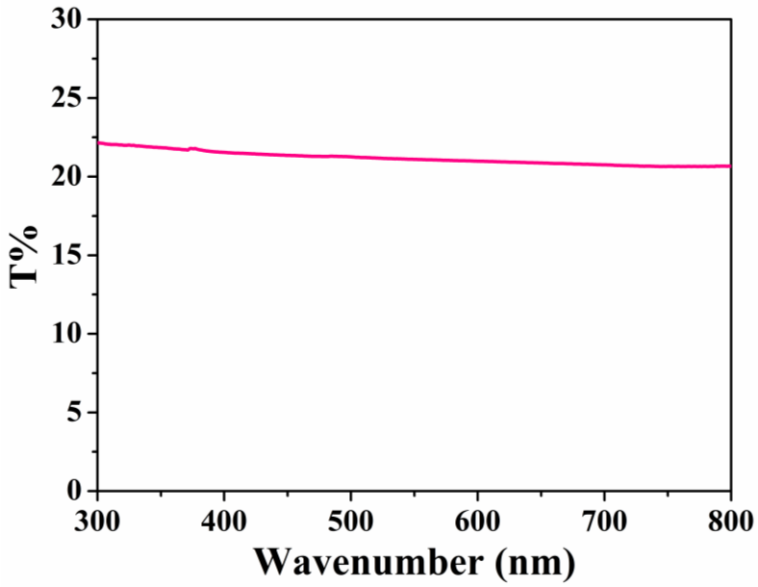

Fig. S30 UV-vis spectra of ZCO NF.

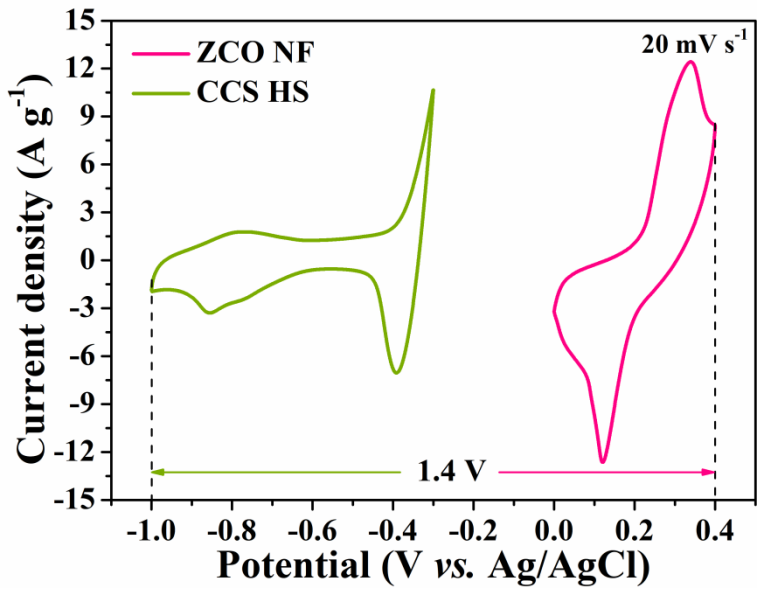

Fig. S31 CV curves of CCS HS and ZCO NF at a scan rate of 20 mV s^{-1}.

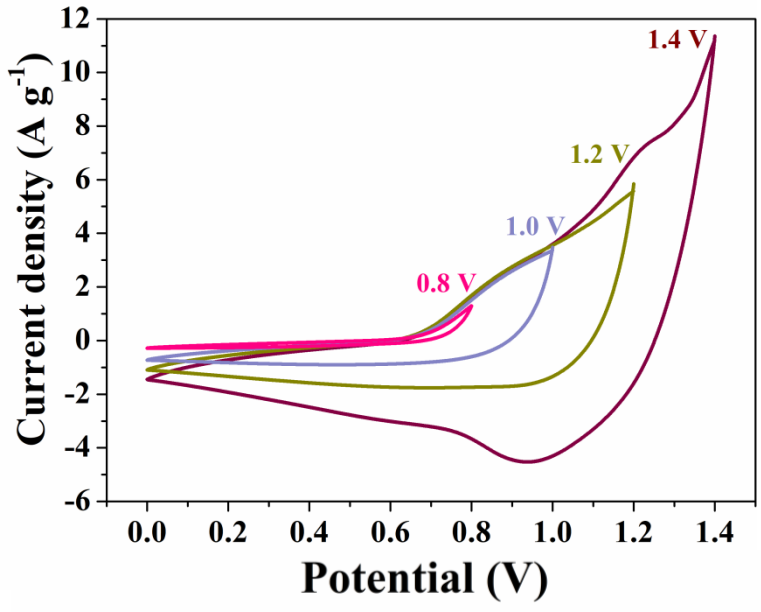

Fig. S32 CV curves of the ZCO NF//CCS HS ASC with the increase of the potential window.

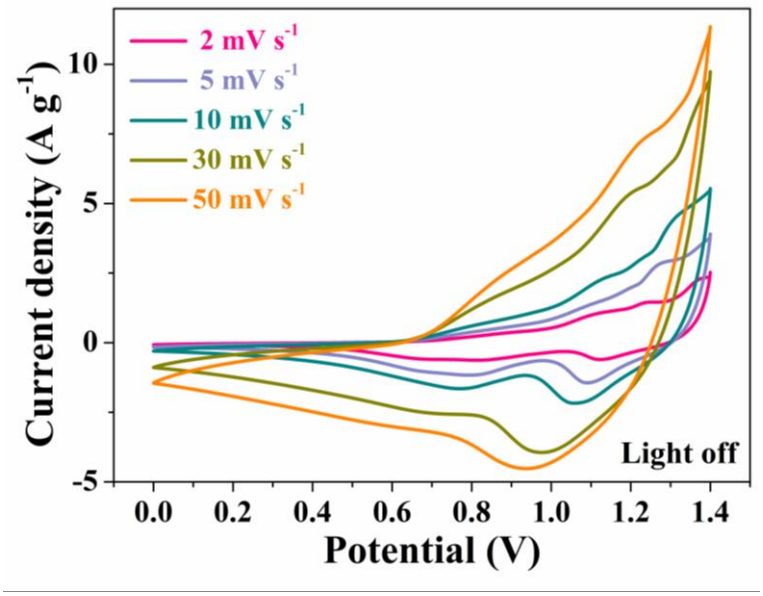

Fig. S33 CV curves for the ZCO NF//CCS HS ASC at different scan rates under dark condition.

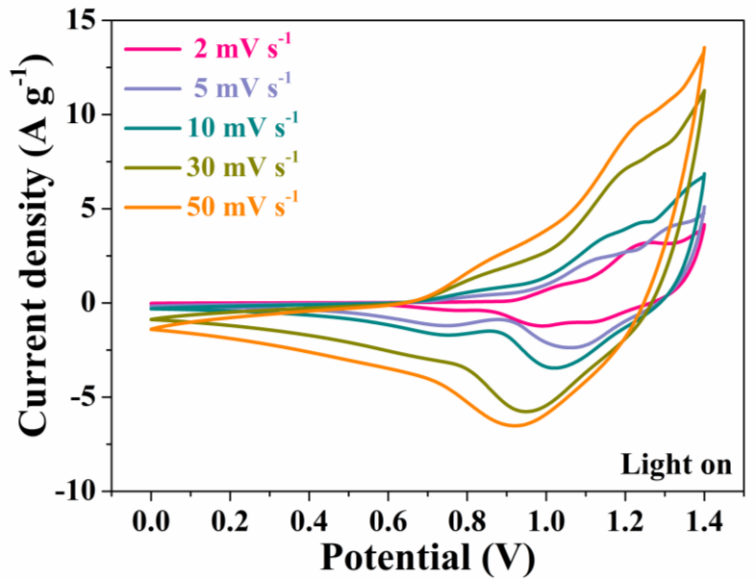

Fig. S34 CV curves for the ZCO NF//CCS HS ASC at different scan rates under light illumination.

Table S4 The specific capacitance of the ZCO NF//CCS HS ASC at various current densities with and without light illumination

	1 A g^{-1}	2 A g^{-1}	3 A g^{-1}	5 A g^{-1}	10 A g^{-1}
Light on	448 F g^{-1} (314 C g^{-1}) (87 mAh g^{-1})	380 F g^{-1} (266 C g^{-1}) (74 mAh g^{-1})	326 F g^{-1} (228 C g^{-1}) (63 mAh g^{-1})	244 F g^{-1} (170 C g^{-1}) (47 mAh g^{-1})	142 F g^{-1} (99 C g^{-1}) (28 mAh g^{-1})
Light off	340 F g^{-1} (238 C g^{-1}) (66 mAh g^{-1})	290 F g^{-1} (203 C g^{-1}) (56 mAh g^{-1})	256 F g^{-1} (180 C g^{-1}) (50 mAh g^{-1})	196 F g^{-1} (135 C g^{-1}) (38 mAh g^{-1})	124 F g^{-1} (87 C g^{-1}) (24 mAh g^{-1})

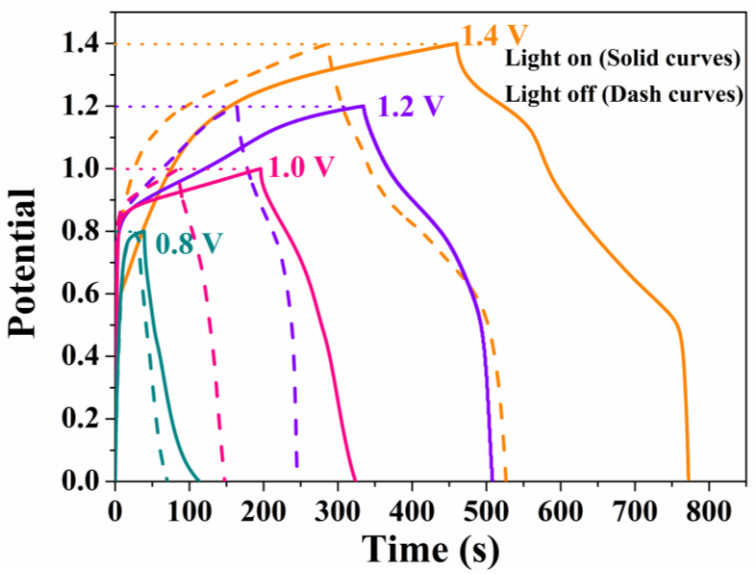

Fig. S35 GCD curves of the ZCO NF//CCS HS ASC at 1 A g^{-1} with the increase of the potential window with and without light illumination.

Table S5 The specific capacitance of the ZCO NF//CCS HS ASC at 1 A g^{-1} with and without light illumination

0-1.4 V		0-1.2 V		0-1.0 V		0-0.8 V	
Light on	Light off	Light on	Light off	Light on	Light off	Light on	Light off
448 F g^{-1}	340 F g^{-1}	291.6 F g^{-1}	134.8 F g^{-1}	254.8 F g^{-1}	127.4 F g^{-1}	184 F g^{-1}	100 F g^{-1}

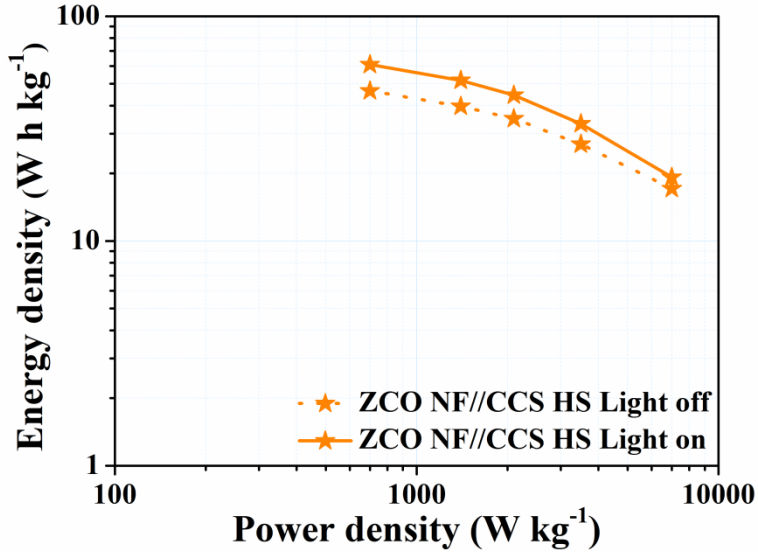

Fig. S36 Ragone plots of the ZCO NF//CCS HS ASC with and without light.

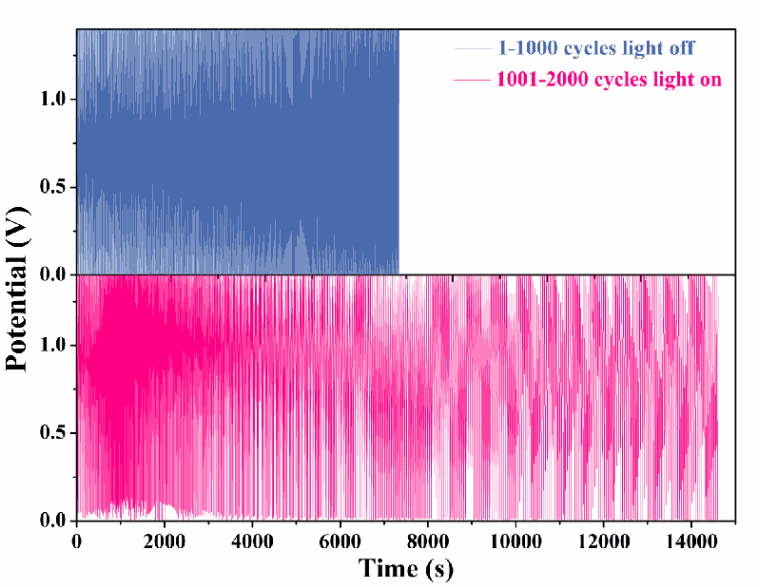

Fig. S37 Photo-response stability of ZCO NF//CCS HS ASC for 2000 cycles.

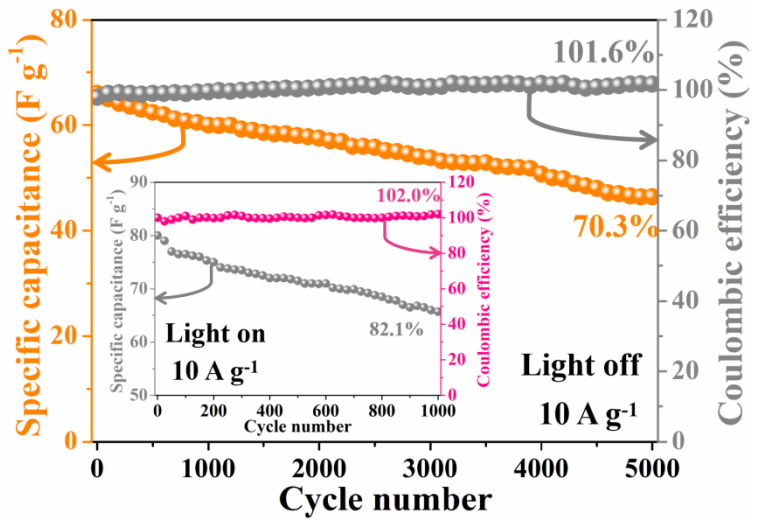

Fig. S38 Cycling stability and coulombic efficiency of the ZCO NF//CCS HS ASC over 5000 cycles at 10 A g^{-1} under dark. Inset shows the cycling stability and coulombic efficiency of the ZCO NF//CCS HS ASC over 1000 cycles at 10 A g^{-1} under light.

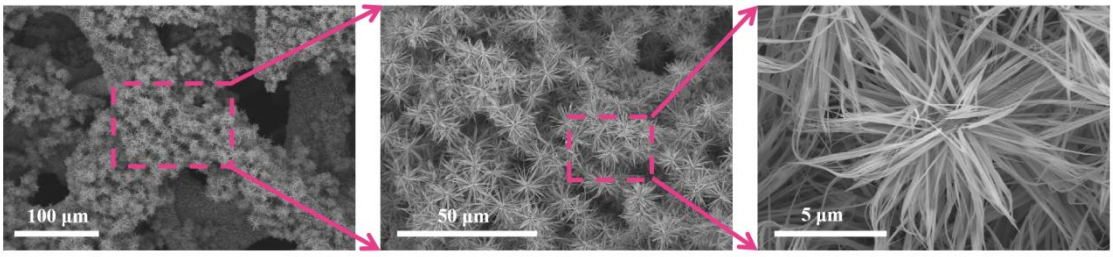

Fig. S39 SEM images of the ZCO NF electrode after cycling.

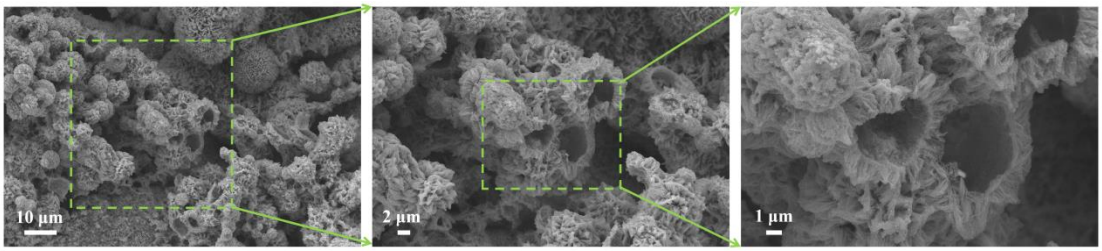

Fig. S40 SEM images of the CCS HS electrode after cycling.

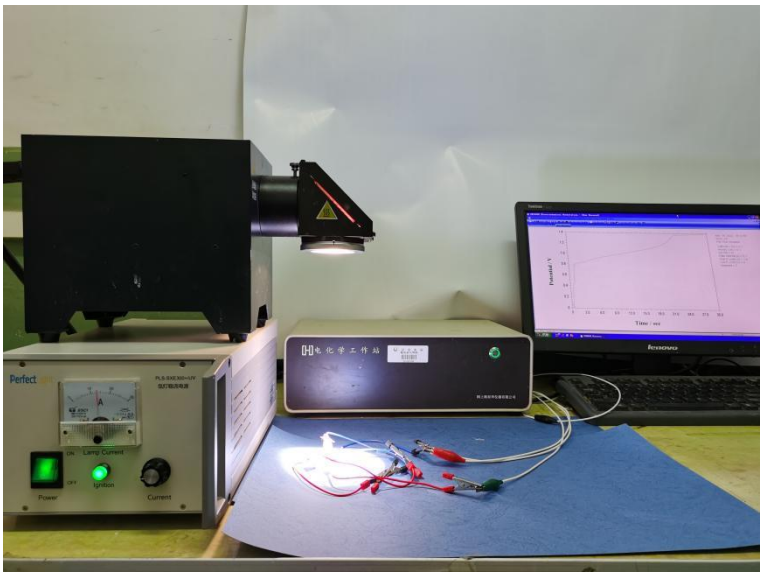

Fig. S41 The charging process of the photo-assisted ZCO NF//CCS HS ASC device.

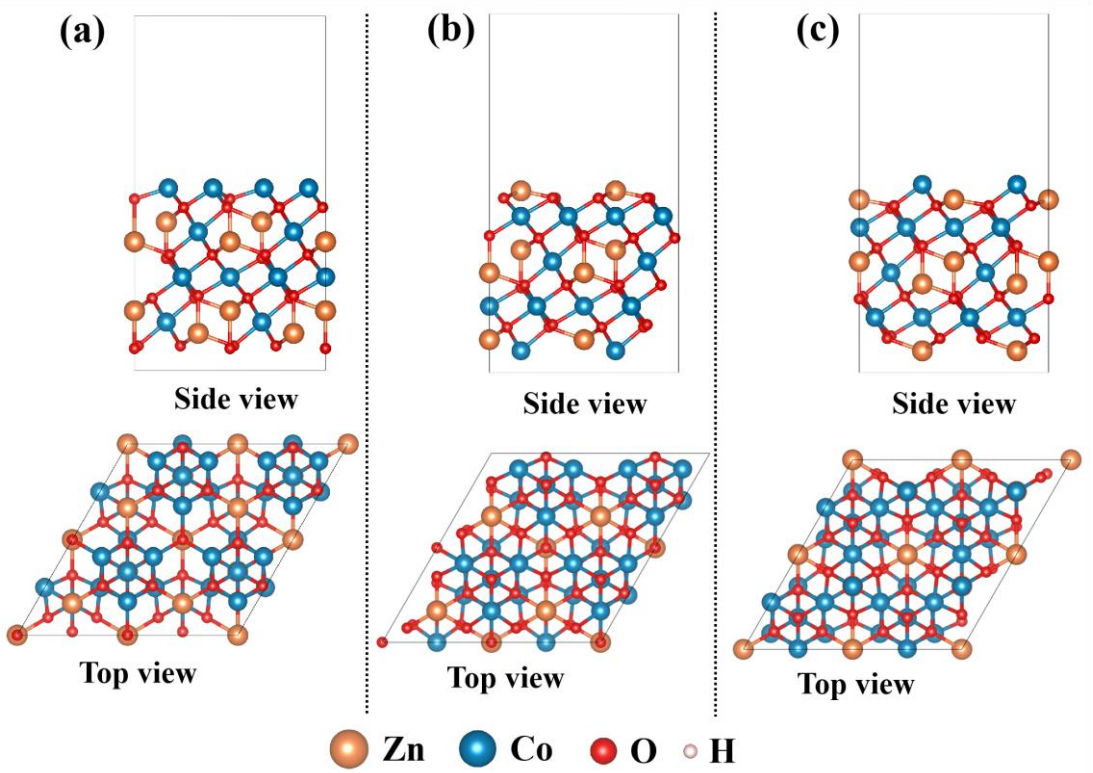

Fig. S42 Optimized geometric structures of $ZnCo_2O_4$ [111] with only exposed Co atoms (a), [111] with only exposed Zn atoms (b) and [111] with exposed Co and Zn atoms (c).

References

[1] W. L. Wu, C. W. Wang, C. H. Zhao, L. Wang, J. F. Zhu, Y. L. Xu, Rational design of hierarchical $FeCo_2O_4$ nanosheets@NiO nanowhiskers core-shell heterostructure as binder-free electrodes for efficient pseudocapacitors, Electrochimica Acta 370 (2021) 137789.

[2] Y. Y. Ling, H. M. Chen, J. J. Zhou, K. Tao, S. H. Zhao, X. B. Yu, L. Han, Metal-Organosulfifide Coordination Polymer Nanosheet Array as a Battery-Type Electrode for an Asymmetric Supercapacitor, Inorganic Chemistry 59 (2020) 7360-7369.

[3] X. R. Lv, L. Chen, X. Q. Min, X. Y. Lin, Y. N. Ni, Flower-like $MnNi_2O_4$-$MnNi_2S_4$ core@shell composite electrode as battery-type supercapacitors, Journal of Energy Storage 55 (2022) 105792.

[4] B. J. Huang, D. C. Yao, J. J. Yuan, Y. R. Tao, Y. X. Yin, G. Y. He, H. Q. Chen, Hydrangea-like $NiMoO_4$-Ag/rGO as Battery-type electrode for hybrid supercapacitors with superior stability, Journal of Colloid and Interface Science 606 (2022) 1652-1661.

[5] N. Zhao, H. Q. Fan, J. W. Ma, M. C. Zhang, C. Wang, H. Li, X. B. Jiang, X. Q. Cao, Entire synergistic contribution of electrodeposited battery-type $NiCo_2O_4$@$Ni_{4.5}Co_{4.5}S_8$ composite for high-performance supercapacitors, Journal of Power Sources 439 (2019) 227097.

[6] Q. Liu, X. D. Hong, X. Y. You, X. Zhang, X. Zhao, X. Chen, M. D. Ye, X. Y. Liu,

Designing heterostructured metal sulfide core-shell nanoneedle films as battery-type electrodes for hybrid supercapacitors, Energy Storage Materials 24 (2020) 541-549.

[7] A. M. Zardkhoshoui, S. S. H. Davarani, Construction of complex copper-cobalt selenide hollow structures as an attractive battery-type electrode material for hybrid supercapacitors, Chemical Engineering Journal 402 (2020) 126241.

[8] S. W. Zhang, B. S. Yin, Y. Z. Luo, L. Shen, B. S. Tang, Z. K. Kou, X. X. Liu, D. B. K. Lim, D. M. Gu, Z. B. Wang, H. Gong, Fabrication and theoretical investigation of cobaltosic sulfide nanosheets for flexible aqueous Zn/Co batteries, Nano Energy 68 (2020) 104314.